Biochimica et Biophysica Acta 1828 (2013) 284–293

Contents lists available at SciVerse ScienceDirect

Biochimica et Biophysica Acta

journal homepage: www.elsevier.com/locate/bbamem

Conformational dynamics and membrane interactions of the *E. coli* outer membrane protein FecA: A molecular dynamics simulation study

Thomas J. Piggot, Daniel A. Holdbrook, Syma Khalid *

School of Chemistry, University of Southampton, Highfield, Southampton, SO17 1BJ, UK

ARTICLE INFO

Article history:
Received 11 May 2012
Received in revised form 2 August 2012
Accepted 23 August 2012
Available online 30 August 2012

Keywords:
Membrane protein
Molecular dynamics
Simulation
Lipopolysaccharide
E. coli
TonB

ABSTRACT

The TonB-dependent transporters mediate high-affinity binding and active transport of a variety of substrates across the outer membrane of *Escherichia coli*. The substrates transported by these proteins are large, scarce nutrients that are unable to gain entry into the cell by passive diffusion across the complex, asymmetric bilayer that constitutes the outer membrane. Experimental studies have identified loop regions that are essential for the correct functioning of these proteins. A number of these loops have been implicated in ligand binding. We report the first simulations of an *E. coli* outer membrane protein in an asymmetric model membrane that incorporates lipopolysaccharide (LPS) molecules. Comparative simulations of the apo and holo forms of the TonB-dependent transporter FecA in different membrane models enable us to identify the nature of the LPS–protein interactions and determine how these interactions impact upon the conformational dynamics of this protein. In particular, our simulations provide molecular-level insights into the influence of the environment and ligand on the dynamics of the functionally important loops of FecA. In addition, we provide insights into the nature of the protein–ligand interactions and ligand induced conformational change in FecA.

1. Introduction

The outer membrane (OM) of gram-negative bacteria is an asymmetric bilayer composed of lipopolysaccharide (LPS) in the outer leaflet and a mixture of zwitterionic and anionic phospholipids in the inner leaflet [1–3]. Transport of nutrients across the OM is typically mediated by pore-forming proteins known as porins. Small molecules and soluble ions passively diffuse through the pores often aided by low affinity binding sites. However, this mechanism of passive diffusion is not adequate for the transport of larger ions and nutrients such as iron and vitamin B_{12}, complexes of which are present in exceedingly small quantities in the extracellular medium under physiological conditions [4]. The problem of the supply of scarce nutrients in sufficient quantities has been resolved by gram-negative bacteria through a sophisticated active transport mechanism involving proteins located in both the OM (transporters) and the inner membrane (the TonB–ExbB–ExbD complex) [5]. TonB-dependent transporters, present in the OM, mediate high affinity binding and active transport of iron-chelating siderophores, vitamin B_{12} and a variety of other substrates [6,7], into the periplasm. Upon entry into the periplasm, these substrates bind to periplasmic proteins and are subsequently transported across the bacterial inner membrane into the cytoplasm [8].

High-resolution X-ray structures of various TonB-dependent transporters have been determined, both in the bound and unbound states. These include the *Escherichia coli* transporters BtuB [9–11], FecA [12,13], FepA [14] and FhuA [15–17]. All of the known structures share a similar topology; they are 22-stranded β-barrels with short stretches of amino acids connecting the β-sheets on the periplasmic side and the long loops on the extracellular side. The β-barrel is occluded by the N-terminal domain (~150 amino acids), which is folded into a globular 'cork' or 'plug' domain. Whilst the exact mechanism of ligand transport remains unknown, it is thought that upon ligand binding a conformational change in the protein allows the binding of the C-terminus of TonB to the periplasmic side of the plug domain [11,12,15–17]. This binding of TonB, in conjunction with energy supplied from the ExbB-ExbD complex, induces a further conformational change in the transporter to allow passage of the ligand through the protein. Several different mechanisms have been proposed for this TonB induced conformational change, including a partial unfolding of the plug domain or a complete exiting of the plug from the β-barrel [18]. Although the exact details are yet to be determined, it is clear that a substantial re-arrangement of this plug domain is required to enable the transport of the solutes through the β-barrel.

The interaction of the TonB-dependent transporters with their local environment is likely to play a significant role in the dynamics and function of the proteins. In particular, residues located within the long extracellular loops are likely to form interactions with the sugars of the LPS outer leaflet through electrostatic and hydrogen-bonding interactions. Indeed, a number of these extracellular loops, which have the potential for interaction with the LPS, have been shown in several mutational and structural studies to be essential in the function of the transporters [19–21]. For example, deletion of loops 3, 7, 8 and 11 of FecA have all

* Corresponding author. Tel.: +44 2380 594176; fax: +44 2380 593781.
E-mail address: S.Khalid@soton.ac.uk (S. Khalid).

0005-2736/$ – see front matter
http://dx.doi.org/10.1016/j.bbamem.2012.08.021

been shown to result in inactive proteins, whilst deletion of loops 5, 9 and 10 showed reduced levels of activity [21]. Some clues regarding the interaction between this family of proteins and the OM environment were also revealed by X-ray structures of FhuA, which showed a LPS molecule bound to FhuA at what has been identified as a putative LPS binding site [15,22]. Thus, we might expect other OMPs of the TonB-dependent transporter family to exhibit similar binding to LPS molecules. Therefore, to study the conformational behaviour of these proteins in an environment that will allow as much of the full complement of interactions with the membrane as is possible given the limitations of simulation timescales, that the protein would experience *in vivo*, it is imperative to consider the asymmetric nature of the outer membrane through inclusion of LPS molecules.

Given that X-ray structures of the TonB-dependent transporters are available in the apo and ligand bound states, with the addition of dynamics to these static structures we can start to build up an understanding of the structure–function relationships of these proteins. In particular we may ask:

1- Do the interactions of these proteins with the outer membrane of *E. coli* play a key role in the protein conformational dynamics?
2- What are the conformational rearrangements that occur when these proteins bind ligands?

To address these questions we have undertaken a molecular dynamics study of apo and holo forms of the *E. coli* TonB-dependent transporter FecA. FecA is responsible for the transportation of the diferric dicitrate (DFDC) siderophore across the *E. coli* OM. The X-ray structures of FecA suggest that the binding of the DFDC ligand induces a conformational change in loops 7 and 8 of FecA to close over the ligand-binding site [12]. In contrast, dicitrate (i.e. two citrate molecules) appears to bind to the protein without inducing a conformational change in FecA [13]. We have employed molecular dynamics simulations to elucidate the impact of ligand binding on the conformational dynamics of FecA. Simulations of FecA were performed in both a simple phosphatidylcholine (PC) membrane and an *E. coli* OM. Our model of the OM, described and validated previously [23], includes Rd_1 LPS molecules [24] in the outer leaflet and a mixture of phosphatidylethanolamine (PE), phosphatidylglycerol (PG) and diphosphatidylglycerol (DPG) (also known as cardiolipin) phospholipids (with common *E. coli* acyl chains) in the inner leaflet (Fig. 1). This represents, to the best of our knowledge, the most detailed membrane reported in molecular dynamics simulation studies of *E. coli* outer membrane proteins (OMPs).

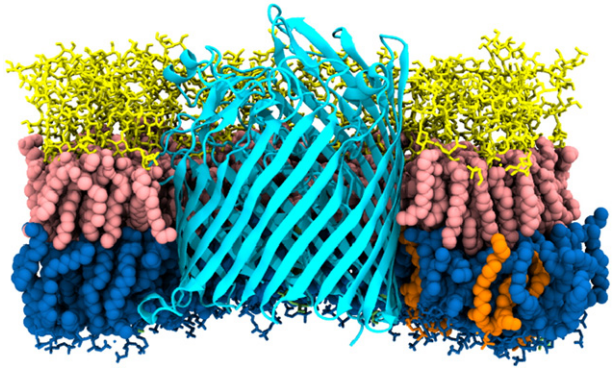

Fig. 1. An image of the FecA Rd_1 LPS/mixed phospholipid OM system. FecA is shown in cyan, LPS acyl chains in pink, LPS sugar and phosphate groups in yellow, PVPE in blue, PVPG in green and PVPV DPG in orange. Water and ions have been omitted for clarity.

2. Methods

2.1. Simulation systems

Table 1 provides a summary of the simulated systems. In total each system contained ~85,000 atoms for the FecA OM simulations and ~115,000 atoms for the FecA PC simulations. The combined length of simulation time was 2.6 μs.

2.2. Simulation protocol

Simulations were performed using the GROMACS package [25–27], version 4.5.1, and the GROMOS 53A6 force field [28] with the SPC water model [29]. Force field parameters for the inner leaflet phospholipids (1-palmitoyl 2-cis-vaccenic phosphatidylethanolamine (PVPE), 1-palmitoyl 2-cis-vaccenic phosphatidylglycerol (PVPG) and 1-palmitoyl 2-cis-vaccenic 3-palmitoyl 4-cis-vaccenic diphosphatidylglycerol (PVPV DPG) [30–32]) and outer leaflet Rd_1 LPS molecules were as we have described and validated previously [23]. Force field parameters for 1-palmityol 2-oleoyl phosphatidylcholine (POPC) were modified from the POPC parameters provided by Kukol [33]. These modified parameters (termed the GROMOS-CKP parameters) are consistent with the inner leaflet phospholipids [23] and substantially improve the properties of POPC membranes [72].

The apo FecA structure was taken from the Protein Data Bank (PDB ID: 1KMO [12]) and missing atoms were added to the structure using the Swiss-PdbViewer, DeepView [34]. Simulations performed with dicitrate and DFDC ligands also used this as a starting structure. The protein was inserted into the equilibrated membranes using the GROMACS programme g_membed [35]. Monovalent (Na^+ or Cl^-) counter-ions, in addition to the Mg^{2+} ions associated with the outer membrane bilayers, were added to neutralise the systems. Energy minimisation was performed using the steepest descent algorithm for 1000 steps to remove any overlapping contacts. A 20 ns simulation, in which the non-hydrogen atoms of the protein were restrained

Table 1
A summary of the simulation systems and the lengths of the simulations.

Name	Lipids	Solvent	Ligand	Simulation length
FecA apo POPC	285 POPC	13 Na^+ 31,088 H_2O	None	3×200 ns[a]
FecA DFDC POPC	285 POPC	13 Na^+ 31,088 H_2O	Diferric dicitrate	2×200 ns
FecA apo OM	58 Rd_1 LPS 130 PVPE 8 PVPG 7 PVPV DPG	323 Mg^{2+} 31 Cl^- 18,919 H_2O	None	2×200 ns
FecA apo OM (D/O)[b]	58 Rd_1 LPS 131 PVPE 8 PVPG 7 PVPV DPG	324 Mg^{2+} 33 Cl^- 18,569 H_2O	None	1×200 ns
FecA citrate OM	58 Rd_1 LPS 130 PVPE 8 PVPG DPG 7 PVPV	323 Mg^{2+} 25 Cl^- 18,913 H_2O	Dicitrate	2×200 ns
FecA DFDC OM	58 Rd_1 LPS 130 PVPE 8 PVPG DPG 7 PVPV	323 Mg^{2+} 31 Cl^- 18,915 H_2O	Diferric dicitrate	2×200 ns
FecA DFDC OM-closed (1KMP)	58 Rd_1 LPS 130 PVPE 8 PVPG DPG 7 PVPV	323 Mg^{2+} 29 Cl^- 18,919 H_2O	Diferric dicitrate	1×200 ns

[a] Two simulations performed using the GROMOS 53A6 force field and one with the GROMOS 54A7 force field.
[b] In this simulation FecA was inserted into the outer membrane bilayer in a different random orientation.

in position, was performed to allow a re-equilibration of the bilayers around the protein. At this point ligands were added as required, using the dicitrate and DFDC positions in structures PDB ID: 1PO0, PDB ID: 1PO3 and PDB ID: 1KMP [12,13] as a guide for their initial location. Upon addition of a ligand, a further 20 ns simulation was performed in which the protein non-hydrogen atoms were restrained in position to allow for an equilibration of the ligand orientation within the binding site. Finally these restraints were removed and a further 200 ns of unrestrained 'production' simulation was performed. Repeat simulations with differently assigned random starting velocities were performed for 200 ns to ensure reproducibility. The Nosé–Hover thermostat [36,37] with a time constant for coupling of 0.5 ps and the Parrinello–Rhaman barostat [38,39] with a time constant for coupling of 5.0 ps were used to maintain a temperature of 313 K and pressure of 1 bar. Electrostatic interactions were treated using the smooth particle mesh Ewald algorithm [40] with a short-range cut-off of 0.9 nm. Van der Waals interactions were truncated at 1.4 nm with a long-range dispersion correction applied to the energy and pressure. The neighbour list was updated every 5 steps during the simulations. All bonds were constrained using the LINCS algorithm [41], allowing a 2 fs timestep to be applied.

2.3. Ligand parameterisation

Parameters for the citrate ligand were assigned using standard GROMOS 53A6 carboxylate and hydroxyl functional group parameters [28]. Parameters for the DFDC ligand were derived using quantum mechanical (QM) calculations performed with the NWChem software [42]. These calculations followed a similar approach to that taken by Kandt et al. for vitamin B_{12} [43]. Geometry optimization was performed at the Hartree–Fock level using the STO-3G basis set, prior to a single-point calculation using the B3LYP [44,45] level of density functional theory with the LANL2DZ basis set [46] used for the iron atoms and the 6-31 +G* basis set used for the non-iron atoms. Atomic partial charges were derived from the electrostatic potential and were symmetrized between ferric citrate molecules. Equilibrium bond lengths and angles were obtained from the QM calculations. Remaining parameters were taken from the GROMOS 53A6 force field [28] and those published by Zinelabidine et al. [47] and Xiao et al. [48].

2.4. General analysis

Analyses were performed using GROMACS tools and locally written code. Statistical tests were performed using the programme R [49]. Details regarding the statistical tests are provided in the Supporting Material. Secondary structure analyses used DSSP [50]. Molecular graphics images were generated using VMD [51].

3. Results

3.1. Structural drift and fluctuations

A comparison of the structural drift of the protein in the simulations from the starting structure provides information regarding its conformational stability and overall conformational motion on the timescale of the simulations. The structural drift was evaluated by calculating the root mean square deviation (RMSD) of the protein loop or β-barrel atoms from the initial ($t=0$) structure as a function of time (Fig. 2 and S1 of the Supporting Material). In all simulations, the RMSD initially rose steadily whilst the system was relaxing, reaching a plateau value by ~50–100 ns. As expected, the β-barrel showed the least deviation (Fig. 2, C and D), whilst the greatest deviation was in the loop regions of the protein (Fig. 2, A and B). Interestingly, differences in the RMSD were observed between the POPC and OM simulations and also between apo, dicitrate and DFDC simulations.

The plateau RMSD values of the loops differed depending upon the membrane environment in which FecA was located. In the POPC simulations the loops RMSD reached a value of ~0.45–0.65 nm, whilst in the OM simulations the loops RMSD reached a value of ~0.30–

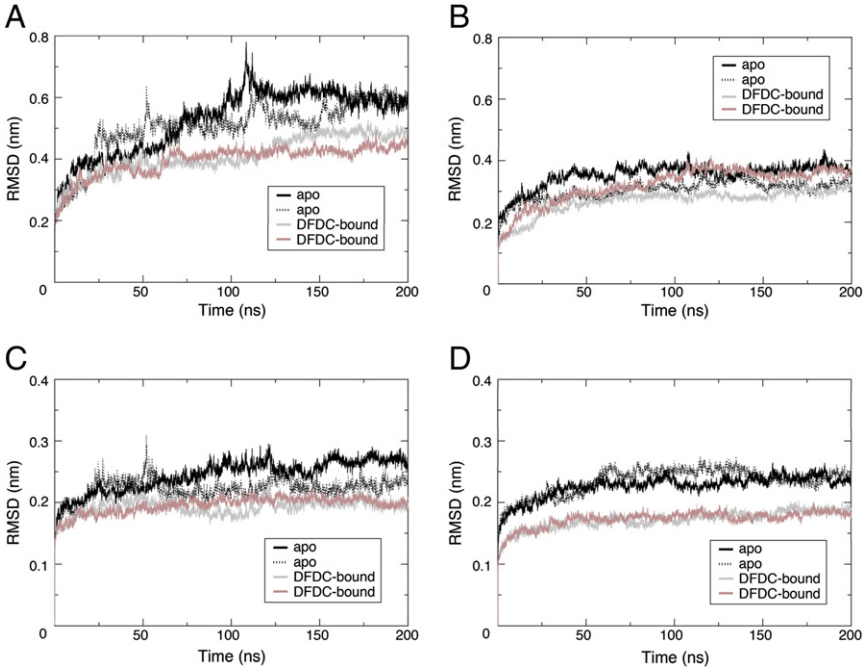

Fig. 2. Root mean square deviations of A) the FecA loops in the POPC membrane, B) the FecA loops in the OM, C) the FecA β-barrel in the POPC membrane and D) the FecA β-barrel in the OM during apo (black solid and dotted lines) and DFDC-bound (grey and brown solid lines) simulations. The loops or β-barrel were fitted, using the least squares method, to the starting conformations prior to the RMSD calculations.

0.40 nm (Fig. 2, A and B; Tables S2 and S3). To ensure that these plateau RMSD values were converged, a block analysis [52] of the RMSD values over the final 50 ns of the simulations was performed. This analysis showed that the standard error of the block means converged for block sizes of >10 ns. In order to visualise the impact of the membrane on the loop dynamics, we calculated the average density for loop Cα atoms from one apo POPC and one apo OM simulation (Fig. 3, A and C). There is an increase in the variability of the conformations that the loops can adopt in the POPC membrane compared to the OM.

The plateau RMSD values of the β-barrel differed depending upon the liganded state of the protein, irrespective of the membrane environment. The RMSD of the β-barrel in the apo and dicitrate bound POPC and OM simulations reached a plateau value of ~0.23–0.28 nm (Fig. 2 and S1). The β-barrel RMSD in the DFDC bound simulations reached a value of ~0.17–0.21 nm (Fig. 2, C and D).

The differences in conformational space explored between simulations can be examined further using all-to-all RMSDs (Fig. 3, B and D). All-to-all RMSDs avoid issues associated with using an arbitrary reference (i.e., starting structure) in the standard RMSD calculation. In particular, whilst differences in plateau RMSD mean that the simulations are sampling different regions of conformational space, similarities in the standard RMSD do not necessarily mean that the simulations are sampling the same region of conformation space [53]. In comparisons of the extracellular loop RMSDs between two POPC simulations there was a large and fast divergence from the starting structure and between simulations, with a maximal RMSD reached of 0.70 nm in 25 ns (Fig. 3 B). In contrast there was little change in RMSD values from the starting configuration or between simulations in the comparisons of two OM simulations, where the loops reached a maximal RMSD of 0.6 nm after 180 ns of simulation, but, thereafter, returned to a configuration more alike the starting configuration, with an RMSD between 0.20 and 0.30 nm (Fig. 3 D). The lower divergence of the loop structures from the starting configuration in OM simulations is clear in all-to-all RMSD plots with POPC simulations (Fig. S2 B). The plots show that the loops in the POPC simulations diverge rapidly from the initial configuration, whilst the loops in OM simulations remain much closer in structure to their original configuration over the whole trajectory, giving the appearance of a gradient across one of the axes in the plot.

The all-to-all plots of the β-barrel RMSDs showed fewer differences between simulations than the plots of the extracellular loops. The largest RMSD between simulations was 0.25 nm, though the RMSDs remained below 0.20 nm in general. The smallest differences in the β-barrel RMSDs were seen in simulations with the bound DFDC ligand, where the RMSDs stayed mostly below 0.15 nm (Fig. S3 A). Furthermore, a gradient in the all-to-all plot can be observed along one of the axis – in similar way, but less strikingly, to the differences between the OM and POPC simulations in the extracellular loop RMSDs – when DFDC simulations are contrasted with apo simulations (Fig. S3 E). This indicates that the ligand may restrict the conformational space explored by the β-barrel.

In order to further explore the influence of the membrane and ligand on the conformational space, we performed a Principal Component Analysis (PCA) on a 1.6 μs trajectory constructed from 8 independent 200 ns trajectories. The PCA was performed on the Cα atoms of both the β-barrel and extracellular loops separately. In both cases the original trajectories were projected onto the first two principal components (Fig. 4). The first two principal components accounted for 30.8% of the total variance in the extracellular loops and 31.1% of the total variance in the β-barrel. The projections indicate that the OM restricts the conformational space of the extracellular loops to a small region on the first two principal components. In contrast, there is a much greater overlap between simulations in the first two principal components of the β-barrel. However, there are three distinct clusters for β-barrel structures, and FecA occupies only one of these clusters when the ligand is bound. The covariance overlap between individual simulations, which takes into account all of the eigenvectors and eigenvalues and not just the first two modes [54–57], shows the same influence of the membrane upon the subspace overlap of the loop motions (Table S1, B and C). There is a minimal impact of the ligand upon the

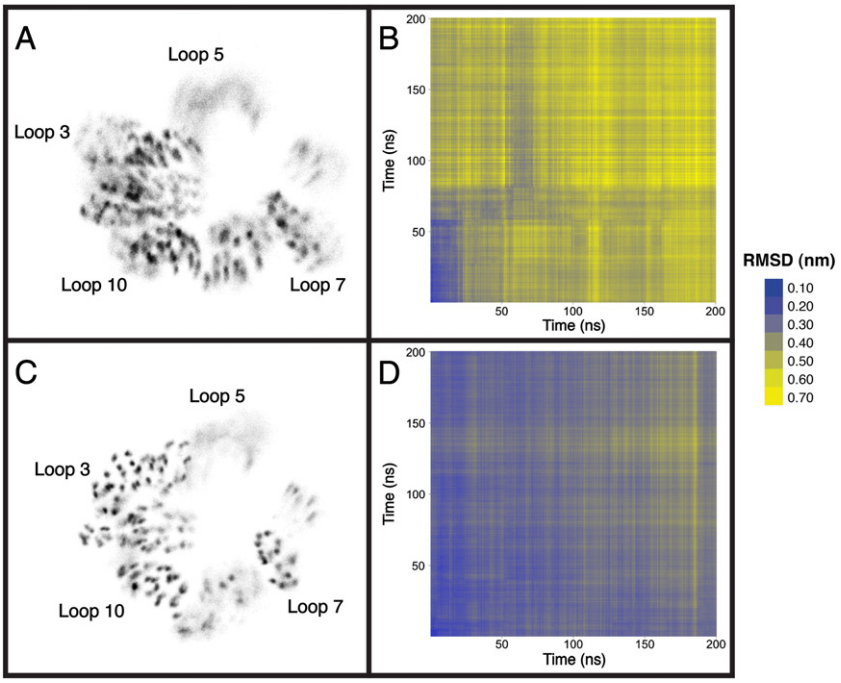

Fig. 3. A top down view of the time averaged density of the Cα atoms from the extracellular loops of FecA for A) POPC and C) OM simulations. The Cα atoms from 400 sample frames were fitted, using the least squares method, to the starting loop conformations. The Cα densities are displayed on a grey scale, where black is high density and white is low density. The levels in this image have been altered equally so that regions with lower Cα densities can be seen more clearly. The differences in loop conformations are also shown in the all-to-all loop RMSD plots of the two apo POPC (B) and the two apo OM (D) simulations. The RMSD colour scale used in B and C is also shown in this figure.

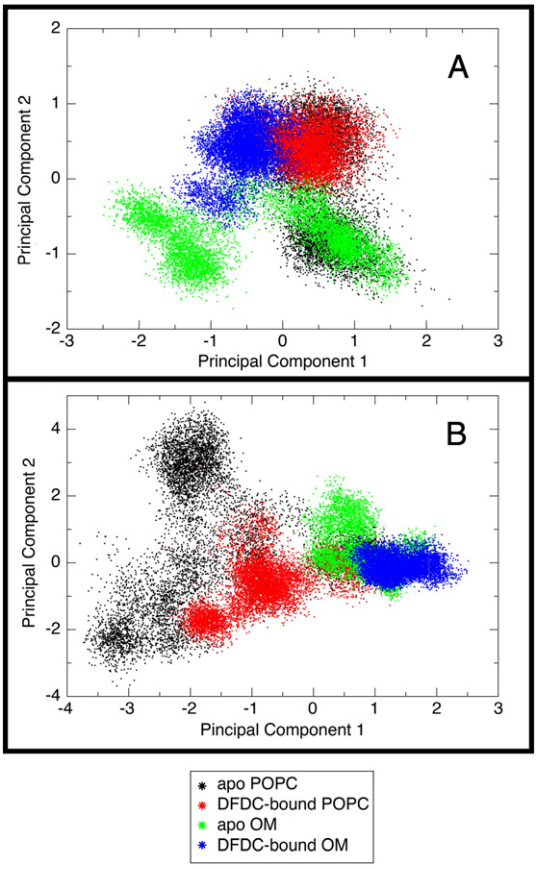

Fig. 4. Projections of the A) barrel and B) loop fluctuations from different simulations on the first two principal components determined from the combined principal component analysis. The apo POPC simulations are shown in black, the apo OM simulations in green, the DFDC-bound POPC simulations in red and the DFDC-bound simulations in blue.

barrel, with a similar covariance overlap in all of the simulations (Table S1 A).

The residue-by-residue fluctuations of the simulated structures, relative to the average structure, provide a measure of the relative flexibility of different regions of the protein. Consistent with the RMSD trends and previous OMP simulations [58–62], the root mean square fluctuations (RMSF) reveal greatest flexibility in the loop regions (Fig. S2). Differences were observed in the loop RMSFs between the POPC and OM FecA simulations; however, no consistent trends in these differences were identified across all the simulations (Fig. S2).

As demonstrated by the RMSD from the initial X-ray derived structure (Fig. 2), the all-to-all RMSD (Fig. 3) and the PCA (Fig. 4), the LPS molecules reduce the overall conformation space sampled by the extracellular loops. This may account for any observed increase in the RMSF values in the POPC compared to OM simulations. To further explore the influence of the LPS on the local fluctuations of the loops we monitored the short-time positional movements of the centre of mass (COM) of the individual FecA loops relative to the Cα atoms in the β-barrel. The longest correlation times for the 50 ps COM movements were determined, from a block analysis, to be <100 ns (Fig. S6 A). In order to remove the influence of the system relaxing, the frames from the first 100 ns were discarded from the start of each trajectory, and the block averaging was repeated for all the loops. In this instance, the longest correlation times for the 50 ps COM movements were <40 ns (Fig. S6 B).

In general, the loop COM movements were lower in the OM than in the POPC membrane (Table S4). The statistical significance of differences in COM loop movements between simulations was evaluated using a two-way analysis of variance (ANOVA). The ANOVA was performed using data averaged over two 50 ns blocks from the final 100 ns of each trajectory. The 50 ns time period was chosen so that the data were average over a time longer than the longest correlation time (Fig. S6). The movements of the loop COM over 50 ps intervals were seen to be significantly different between the POPC and OM simulations at the 5% level for extracellular loop 4 ($p=0.015$), loop 5 ($p=0.016$) and loop 6 ($p=0.012$) and at the 1% level for loop 1 ($p<0.001$), loop 2 ($p=0.002$), loop 3 ($p<0.001$), loop 7 ($p=0.006$), loop 8 ($p=0.004$), loop 9 ($p<0.001$), loop 10 ($p<0.001$) and loop 11 ($p=0.001$) (Table S5). The ligand also had a statistically significant effect at the 5% level on loop 5 ($p=0.039$) and loop 9 ($p=0.039$) and at the 10% level on loop 11 ($p=0.055$). These results indicate that differences in membrane environment and, to a lesser extent, binding of the DFDC ligand can significantly alter the fast fluctuations of the FecA loops relative to the β-barrel.

3.2. Protein–membrane interactions

To identify the factors that influence the observed differences in conformational dynamics of FecA in the two different membranes, it is important to consider its interaction with the surrounding environment. We monitored various protein–lipid interactions, where interaction is defined as protein–lipid distance ≤0.35 nm (Fig. 5 and S7). A similar pattern of interactions was observed between FecA and the POPC lipid head groups to that previously reported from simulations of OMPs in symmetric phospholipid bilayers [63]. The trends were also reproduced between FecA and the inner leaflet phospholipids of the OM bilayer. In contrast, a substantial number of interactions occurred between the LPS sugar and phosphate groups and extracellular regions of the protein that were not observed in the POPC bilayer simulations (Fig. 5 and S7). The protein residues predominantly formed

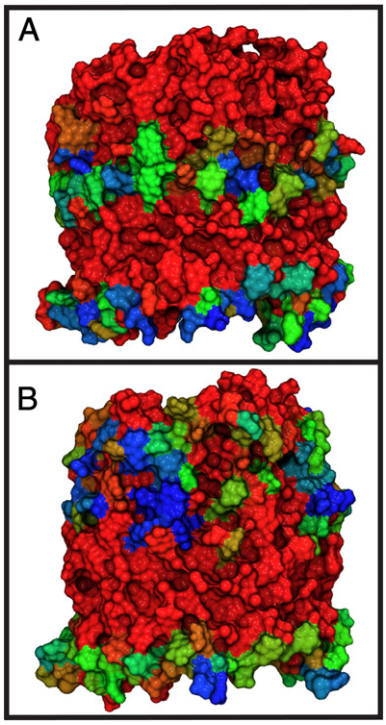

Fig. 5. Protein–membrane interactions during an A) POPC and B) OM simulation. An interaction is defined as any protein and LPS, PVPE, PVPG, PVPV DPG or POPC head group atoms that are within 0.35 nm. The proteins are coloured on a red–green–blue colour scale. Red means that there are no interactions during the simulations whilst blue means an interaction is formed for 100% of the simulation.

hydrogen-bonding interactions to the LPS molecules. Electrostatic interactions between charged residues and LPS phosphate and carboxylate moieties were observed infrequently.

To highlight the nature of the interactions between the loops of FecA and the environment, we will focus on the interactions between loop 3 (residues 310 to 330) and the Rd_1 LPS molecules. In mutational studies this loop has been shown to be essential in the function of FecA, with deletions of this loop leading to an inactive protein [21]. This example typifies the interactions that are formed between the FecA loops and the LPS inner core sugars during the OM simulations. Interactions between residues of loop 3 (especially D322, R323 and Q325) and Rd_1 LPS molecules occurred throughout the simulations (Fig. 6). These residues did not exhibit interactions to the lipids in the POPC bilayer simulations. In the OM simulations, residues D322 and Q325 were often orientated such that their side chains point towards the same two Rd_1 LPS molecules, forming hydrogen bonds to hydroxyl groups of the LPS heptose sugars (Fig. 6 B). Residue R323 also exhibited a propensity to form hydrogen-bonding interactions with sugars of LPS molecules (Fig. 6 C). Details regarding the occupancies of these protein–lipid hydrogen-bonding interactions for the OM simulations are provided in Table 2. To further highlight the nature of these interactions the minimum distances between these three residues and the LPS molecules for one apo FecA OM simulation are shown in Fig. 6 D. Individual hydrogen-bonding interaction events were fairly transient, with typical lifetimes of <50 ps. However, as indicated by the occupancies (Table 2), these interactions were frequently formed throughout the simulations. This one example of loop 3 typifies the nature of the interactions formed between polar and charged residues in other loops of the protein and the LPS sugars.

In addition to interactions between the inner core sugars of the LPS and extracellular loops of FecA, differences were observed in the pattern of interactions between the protein and the two leaflets of the membranes. The relatively small size and fast diffusion of the inner leaflet phospholipids enabled electrostatic and hydrogen-bonding interactions between the phospholipid head groups with most residues on the periplasmic side of the protein (Fig. 5 and S7). In contrast, the bulky and slower diffusing LPS molecules were unable to move to interact with small residues at the extracellular hydrophobic/hydrophilic interfacial region of FecA. However, bulkier residues, such as tryptophan, glutamine, arginine and lysine, were able to form interactions with LPS molecules in these regions (Fig. 5 and S7).

Table 2
The occupancies of the hydrogen-bond interactions (i.e. the percentage of simulation time the hydrogen-bonds are formed) between residues Asp 322, Arg 323, Gln 325 and the LPS molecules during the OM simulations. The values are averaged over any repeat simulations performed (see Table 1 for further details of the simulations).

Simulation	Occupancy (%)		
	Asp 322	Arg 323	Gln 325
FecA apo OM	39.9	6.8	42.4
FecA apo OM (D/O)	34.4	51.2	0
FecA Citrate OM	48.7	11.5	29.8
FecA DFDC OM	95.2	33.6	35.1
FecA DFDC OM-closed	27.4	23.8	15.4

3.3. Protein–ligand interactions

The results presented earlier indicate that the DFDC ligand may influence the β-barrel, and to a lesser extent, the loop dynamics. To further investigate the effects of the ligands we monitored the movement and interactions of the ligand during both sets of DFDC-bound and dicitrate-bound simulations. Somewhat surprisingly, both dicitrate and DFDC ligands were able to move away from the ligand binding site during the simulations (Fig. 7 and S8). To quantify the extent of movement of the ligands, the RMSD of the ligands was calculated with respect to the protein atoms (Fig. 6 C and S8 C). The dicitrate ligand was initially

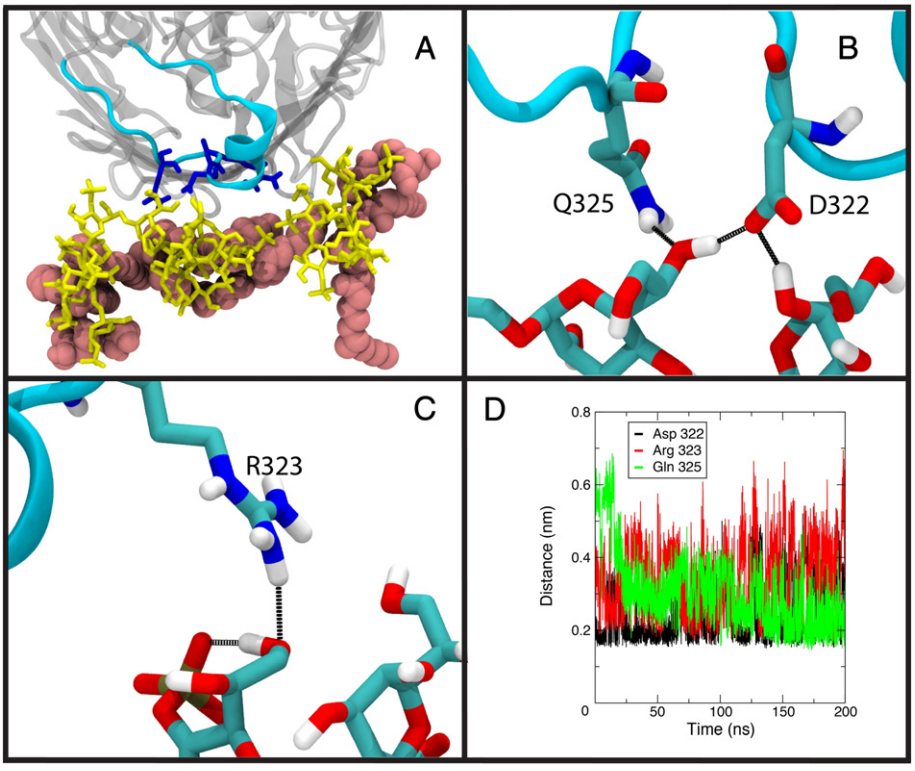

Fig. 6. A) A top down image highlighting the interaction of loop 3 of FecA and three LPS molecules. B) An image of the hydrogen bond interactions of Asp 322 and Gln 325 with two LPS molecules. C) An image of the hydrogen bond interaction of Arg 323 and the sugars of an LPS molecule. D) The minimum distances between Asp 322 (black), Arg 323 (red), Gln 325 (green) and the LPS molecules during an OM simulation.

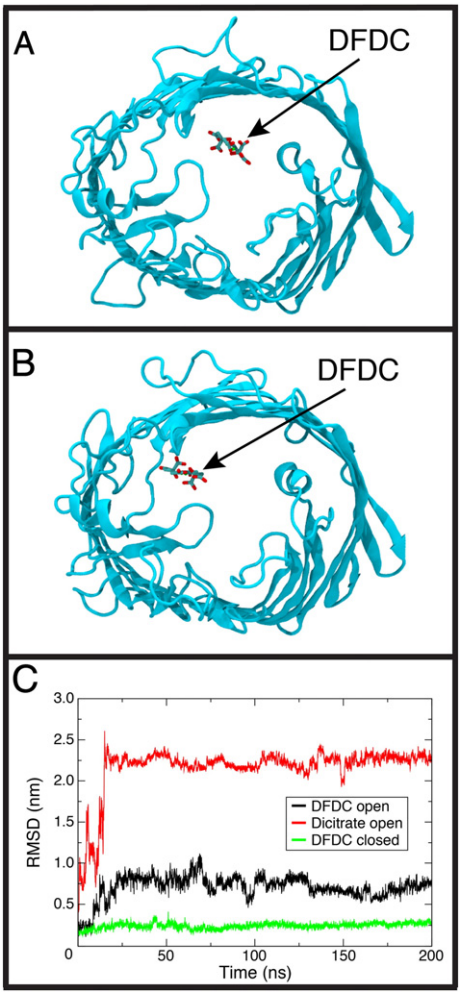

Fig. 7. Top down view of FecA showing the A) initial and B) final positioning of DFDC within the protein. The plug domain in these images has been removed for clarity. C) The RMSD of the ligands with the protein residues fitted, using the least squares method, to the starting conformation. The RMSD of DFDC initially located in the open FecA binding site is shown in black, the RMSD of dicitrate initially located in the open FecA binding in red and DFDC initially located in the closed FecA binding site in green.

the most mobile, as indicated by the large increase in RMSD to a plateau value of ~2.25 nm with respect to the protein, over the first ~20 ns. This increase in RMSD corresponds to one of the citrate molecules completely escaping from the protein during this dicitrate-bound simulation (Fig. S8 A). In general, the movement of DFDC was towards loops 11, 3 and 4 of FecA (Fig. S9), although there was some variability in the direction of movement. In particular, in one of the POPC DFDC-bound simulations, the movement of the ligand was in the opposite directions towards loops 7 and 8 (Fig. S9 D). In the three simulations where the ligand moved towards loops 11, 3 and 4, electrostatic interactions were often formed between DFDC and residues located in these loops and neighbouring strands of the β-barrel. In particular interactions were frequently formed between the carboxylate groups of DFDC and residues Arg 328, Gln 371, Asn 721 and Asn 722 (Fig. S9 A–C). In contrast to this mobility of DFDC in simulations performed with the ligand placed into the open binding site of the apo FecA structure, there was a substantially reduced mobility of the DFDC ligand in simulations performed using the DFDC-bound FecA structure PDB ID: 1KMP (Fig. 7 C and S8 B). This reduction in movement was due to DFDC interactions with loop 8; this loop is closed over the ligand binding in this X-ray structure. In particular, in agreement with experimental predictions [21], the carboxylate groups of DFDC formed interactions with Gln 570 of loop 8 (Fig. S8 D).

3.4. Barrel interior: plug domain dynamics

Having established the relative flexibilities of the different regions of the proteins in the two different membranes, and the nature of the ligand–protein interactions, from a functional perspective it is of interest to examine the properties of the β-barrel interior in greater detail. The position of the plug domain within the β-barrel did not alter substantially during the simulations (e.g., Fig. 8 A). The integrity of the secondary structure of the plug domain was maintained throughout the simulations (Fig. 8). The exception to the limited change in conformation was in the secondary structure of one of the α-helices in the plug domain. This H1 helix (residues 94–100), also known as the 'switch helix', unfolded in all the simulations (apart from the simulation started from the PDB ID: 1KMP X-ray structure in which this helix is already unfolded) (Fig. 8 and S10). This is particularly interesting as it has been suggested from experimental work that the unfolding of this helix only occurs upon ligand binding to FecA [12]. To ensure that this unwinding was not an artefact of the inherent instability of small helices using the GROMOS 53A6 force field [64], an additional simulation was performed using the recently updated GROMOS 54A7 force field [64,65] for the protein and the same POPC model. In agreement with the GROMOS 53A6 simulations, the H1 switch helix unfolded during this simulation (Fig. S10 J). The unfolding of the switch helix was often of a reversible nature, with transient unfolding and refolding of the helix occurring in several of the 200 ns simulations (Fig. 8 and S10).

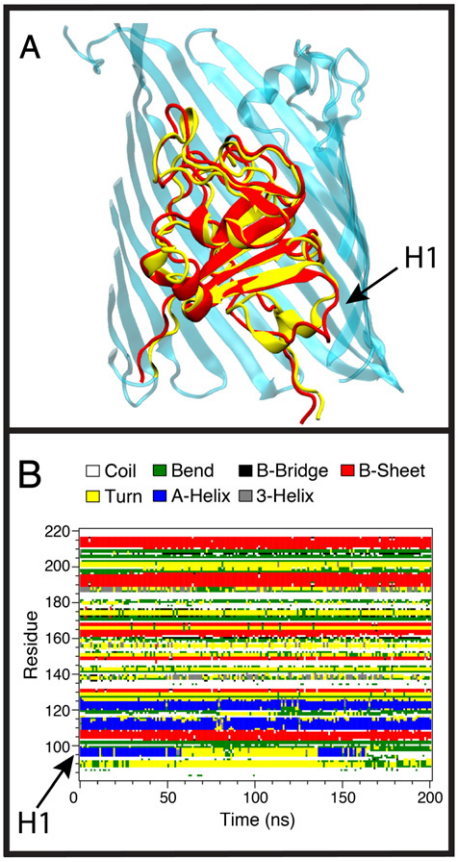

Fig. 8. A) Initial (yellow) and final (red) conformations of the FecA plug domain from an apo OM simulation. The location of the H1 switch helix is shown in the Fig. B) The secondary structure of the FecA plug domain during an apo OM simulation. The region corresponding to the H1 switch helix (residues 94–100) is highlighted in the figure.

4. Discussion and conclusion

We have performed molecular dynamics simulations of the TonB-dependent transporter FecA in the apo and two different bound states, within two different membrane models. The discussion of our results is divided into two sections for clarity.

4.1. Interactions with the surrounding membrane

Simulations performed of FecA in POPC and OM bilayers have illuminated details regarding the nature of the interactions between this OMP and the membrane environment. A substantial number of interactions were observed between the inner core sugars of the LPS molecules and extracellular residues of the protein that were not observed in the POPC simulations. Typically these interactions involved residues in the loops of the protein and were hydrogen-bonding interactions. Electrostatic interactions between charged residues and the charged groups of the LPS were only infrequently formed. Presumably the interaction of the LPS phosphate and carboxylate groups with Mg^{2+} ions in the OM, in addition to the formation of intra- and inter-molecular LPS hydrogen bonds [23], reduces the likelihood of electrostatic interactions between the protein and the LPS. Analysis of the conformational stability of the protein in both membrane environments revealed that the interactions between protein and LPS had a significant impact upon the loop dynamics. The interactions significantly altered the short-term fluctuations in loop position, and the interactions also altered the longer-term conformations that could be adopted by the loops. It appears that the impact of the LPS upon loop dynamics arises *via* two different mechanisms. Short-lived but frequently formed non-specific hydrogen-bonding interactions alter the local fluctuations in loop movement, whilst the bulky LPS molecules provide a steric resistance to larger conformational motions of the loops. These results highlight the need for complex membrane models when exploring the conformational dynamics of these long extracellular loops. The only previously published simulation of an OMP in a membrane incorporating LPS was a study of OprF, an OMP from *Pseudomonas aeruginosa* [66]. A comparison of simulations performed in an asymmetric OM and simulations of OprF performed in a PC membrane [67] suggested that the LPS influenced the protein RMSDs, the RMSD equilibration time and a specific loop RMSF. Whilst there is some agreement with the results presented here and those presented in this previous study (e.g., loop RMSDs), differences in the OM models and proteins studied are likely to contribute to some of the observed differences in the results. Additionally, the shorter simulation time (10 ns) and fewer numbers of simulations (only 2) also likely provide an explanation for some of the differences observed.

It is useful to reflect upon some methodological limitations of the current study regarding interactions with the OM. We note that due to the slow diffusion rate of LPS, any specific protein–LPS interactions are to some extent influenced by aspects of the initial simulation setup, such as the positioning of the protein within the membrane. Encouragingly, a simulation in which FecA was inserted into the OM in a different random orientation showed the same trends in membrane interaction as the original FecA OM simulations (Fig. S11). In the present study, having run multiple independent simulations of each system for 200 ns, we have a reasonable level of sampling. However, with longer simulations we expect the differences between environments to become more apparent through an increase the number of independent data points used in the statistical analyses. Future studies would benefit from running these longer simulations, with a greater number of repeat simulations, and perhaps also employing accelerated sampling techniques such as metadynamics [68]. In addition to problems regarding the slow moving nature of the LPS molecules, the observed influence of the LPS on the protein dynamics may well differ for different OMPs and with different levels of LPS. For example, it is possible that increased levels of LPS (to include the outer core and O-antigen) may further impact upon the conformational dynamics of the FecA loops. Specifically, we speculate that the dynamics of loop 5 may be further altered with full rough and smooth LPS, given its location and orientation.

4.2. Ligand induced conformational change

The conformational changes that occur upon ligand binding to the TonB-dependent transporters are keys to the function of these proteins. In particular we may ask: how does siderophore binding in the extracellular side of the transporter regulate binding activities at the periplasmic surface? Whilst the precise chain of conformational changes that occur are yet to be fully characterised, X-ray structures of FecA suggest that upon DFDC binding: (i) loops 7 and 8 undergo a conformational change so as to close over the DFDC binding site and (ii) the H1 switch helix of the plug domain unwinds. This unwinding of the switch helix has been suggested to facilitate the binding of TonB to the TonB box of the plug domain [12]. It has also been suggested from crystallography experiments that prior to DFDC binding, two citrate molecules occupy the ligand binding site and these are displaced upon ligand binding [13]. The results presented in this work provide further insights into potential mechanism of ligand induced conformational change in this protein and challenge some of these previous hypotheses.

The occupation of the open binding site with two citrate molecules is somewhat unlikely, given the mobility of the citrate molecules when initially placed into the binding site. This is further highlighted by the fact that even over the relatively short timescales of the simulations it is possible for citrate molecules to completely leave the protein and move to interact with the LPS molecules of the OM. Simulations of FecA with DFDC located in the open binding site also revealed movements of the ligand within the protein. The DFDC ligand did not induce a conformational change in loops 7 and 8 to close over the binding site over the timescales of the simulations, rather the ligand moved to interact with other parts of the protein. This is in contrast to previously published simulations of another TonB-dependent transporter, FhuA, where a fairly rapid movement of loop 8 to cover the ligand-binding site was observed in the ligand-bound simulations [59]. Therefore, the simulations presented in this work suggest potential differences in the mechanisms and timescales of loop closure in these two proteins. This observation is in agreement with experimental work that has shown that these loops are likely to function in different ways in FecA and FhuA. FecA loop 8 deletion mutants have been shown to remove all FecA activity [21], whilst loop 8 mutants in FhuA exhibit normal activity [19]. Perhaps, as has been suggested experimentally [21], the DFDC ligand binds to a different part of the protein prior to loop closure. Interestingly, interactions of the DFDC ligand with the β-barrel and loops appear to influence the dynamics of the protein. This observation may have functional implications for the protein. For example, the β-barrel may need to be stabilized before the large-scale conformational changes in the plug domain can occur, which ultimately allow the ligand to pass through the protein. Simulations starting from the closed structure of FecA reveal a reduced movement of the ligand, with the ligand remaining in the binding site. Secondary structure analysis of the plug domain during the simulations shows that in both apo and holo forms of the open FecA structure, the switch helix is able to unfold and refold on the 200 ns timescale of the simulations. This is consistent with the experimental observation, which, in contrast to the X-ray structures, suggests that upon ligand binding to FecA there is no concerted conformational change in the switch helix [69]. Presumably during the crystallization process the folded conformation of the switch helix is favoured, which is why in the X-ray structures of apo FecA the switch helix is folded.

Overall our results have revealed conformational rearrangements of FecA in the loop regions and also unwinding of the switch helix. Our simulations show that interaction with LPS molecules in the

outer leaflet of the OM has a significant influence on the loop dynamics of FecA. Experimental validation e.g., NMR [70] or ESR [71] studies of the differences in the dynamics of FecA in the asymmetric membrane compared to the purely phospholipid one, would be desirable in extending this study in the future. Given the structural and functional similarities between FecA and other TonB-dependent transporters from *E. coli*, we might expect such membrane–protein interactions to play a key role in their dynamics too. In general it would be of interest to extend the current study, in which the heterogeneity of the OM lipids is incorporated, to not only other TonB-dependent transporters, but also other OMP families. Such simulations have the potential to bridge the gap in complexity between experimental studies, which are often conducted in model membrane systems, and *in vivo* functional studies.

Acknowledgements

This work was supported by a grant from the BBSRC (BB/H000658/1). SK is an RCUK fellow. We thank Stephen Fox and Marc Baaden for their help with the DFDC ligand parameterisation. We also thank Tjerk Straatsma, Joseph Goose and Mark Sansom for the helpful discussions and sharing of expertise. We wish to acknowledge the use of the IRIDIS High Performance Computing Facility at the University of Southampton.

Appendix A. Supplementary data

Supplementary data to this article can be found online at http://dx.doi.org/10.1016/j.bbamem.2012.08.021.

References

[1] E.J.J. Lugtenberg, R. Peters, Distribution of lipids in cytoplasmic and outer membranes of *Escherichia coli* K12, BBA - Lipid Lipid Metab. 441 (1976) 38–47.
[2] M.J. Osborn, Structure and biosynthesis of the bacterial cell wall, Annu. Rev. Biochem. 38 (1969) 501–538.
[3] C.R. Raetz, Enzymology, genetics, and regulation of membrane phospholipid synthesis in *Escherichia coli*, Microbiol. Mol. Biol. Rev. 42 (1978) 614–659.
[4] K.N. Raymond, E.A. Dertz, S.S. Kim, Enterobactin: an archetype for microbial iron transport, Proc. Natl. Acad. Sci. 100 (2003) 3584–3588.
[5] V. Braun, M. Braun, Iron transport and signaling in *Escherichia coli*, FEBS Lett. 529 (2002) 78–85.
[6] D.P. Chimento, R.J. Kadner, M.C. Wiener, Comparative structural analysis of TonB-dependent outer membrane transporters: implications for the transport cycle, Proteins 59 (2005) 240–251.
[7] N. Noinaj, M. Guillier, T.J. Barnard, S.K. Buchanan, TonB-dependent transporters: regulation, structure, and function, Annu. Rev. Microbiol. 64 (2010) 43–60.
[8] S.C. Andrews, A.K. Robinson, F. Rodríguez-Quiñones, Bacterial iron homeostasis, FEMS Microbiol. Rev. 27 (2003) 215–237.
[9] V. Cherezov, E. Yamashita, W. Liu, M. Zhalnina, W.A. Cramer, M. Caffrey, In meso structure of the cobalamin transporter, BtuB, at 1.95 Å resolution, J. Mol. Biol. 364 (2006) 716–734.
[10] D.P. Chimento, A.K. Mohanty, R.J. Kadner, M.C. Wiener, Substrate-induced transmembrane signaling in the cobalamin transporter BtuB, Nat. Struct. Mol. Biol. 10 (2003) 394–401.
[11] D.D. Shultis, M.D. Purdy, C.N. Banchs, M.C. Wiener, Outer membrane active transport: structure of the BtuB:TonB complex, Science 312 (2006) 1396–1399.
[12] A.D. Ferguson, R. Chakraborty, B.S. Smith, L. Esser, D. van der Helm, J. Deisenhofer, Structural basis of gating by the outer membrane transporter FecA, Science 295 (2002) 1715–1719.
[13] W.W. Yue, S. Grizot, S.K. Buchanan, Structural evidence for iron-free citrate and ferric citrate binding to the TonB-dependent outer membrane transporter FecA, J. Mol. Biol. 332 (2003) 353–368.
[14] S.K. Buchanan, B.S. Smith, L. Venkatramani, D. Xia, L. Esser, M. Palnitkar, R. Chakraborty, D. van der Helm, J. Deisenhofer, Crystal structure of the outer membrane active transporter FepA from *Escherichia coli*, Nat. Struct. Mol. Biol. 6 (1999) 56–63.
[15] A.D. Ferguson, E. Hofmann, J.W. Coulton, K. Diederichs, W. Welte, Siderophore-mediated iron transport: crystal structure of FhuA with bound lipopolysaccharide, Science 282 (1998) 2215–2220.
[16] K.P. Locher, B. Rees, R. Koebnik, A. Mitschler, L. Moulinier, J.P. Rosenbusch, D. Moras, Transmembrane signaling across the ligand-gated FhuA receptor: crystal structures of free and ferrichrome-bound states reveal allosteric changes, Cell 95 (1998) 771–778.
[17] P.D. Pawelek, N. Croteau, C. Ng-Thow-Hing, C.M. Khursigara, N. Moiseeva, M. Allaire, J.W. Coulton, Structure of TonB in complex with FhuA, *E. coli* outer membrane receptor, Science 312 (2006) 1399–1402.
[18] K.D. Krewulak, H.J. Vogel, TonB or not TonB: is that the question? Biochem. Cell Biol. 89 (2011) 87–97.
[19] F. Endriß, V. Braun, Loop deletions indicate regions important for FhuA transport and receptor functions in *Escherichia coli*, J. Bacteriol. 186 (2004) 4818–4823.
[20] C.A. Fuller-Schaefer, R.J. Kadner, Multiple extracellular loops contribute to substrate binding and transport by the *Escherichia coli* cobalamin transporter BtuB, J. Bacteriol. 187 (2005) 1732–1739.
[21] A. Sauter, V. Braun, Defined inactive FecA derivatives mutated in functional domains of the outer membrane transport and signaling protein of *Escherichia coli* K-12, J. Bacteriol. 186 (2004) 5303–5310.
[22] A.D. Ferguson, W. Welte, E. Hofmann, B. Lindner, O. Holst, J.W. Coulton, K. Diederichs, A conserved structural motif for lipopolysaccharide recognition by procaryotic and eucaryotic proteins, Structure 8 (2000) 585–592.
[23] T.J. Piggot, D.A. Holdbrook, S. Khalid, Electroporation of the *E. coli* and *S. aureus* membranes: molecular dynamics simulations of complex bacterial membranes, J. Phys. Chem. B 115 (2011) 13381–13388.
[24] C.R.H. Raetz, Biochemistry of endotoxins, Annu. Rev. Biochem. 59 (1990) 129–170.
[25] H.J.C. Berendsen, D. van der Spoel, R. van Drunen, GROMACS: a message-passing parallel molecular dynamics implementation, Comput. Phys. Commun. 91 (1995) 43–56.
[26] D. van der Spoel, E. Lindahl, B. Hess, G. Groenhof, A.E. Mark, H.J.C. Berendsen, GROMACS: fast, flexible, and free, J. Comput. Chem. 26 (2005) 1701–1718.
[27] B. Hess, C. Kutzner, D. van der Spoel, E. Lindahl, GROMACS 4: algorithms for highly efficient, load-balanced, and scalable molecular simulation, J. Chem. Theory Comput. 4 (2008) 435–447.
[28] C. Oostenbrink, A. Villa, A.E. Mark, W.F. van Gunsteren, A biomolecular force field based on the free enthalpy of hydration and solvation: the GROMOS force-field parameter sets 53A5 and 53A6, J. Comput. Chem. 25 (2004) 1656–1676.
[29] H. Berendsen, J. Postma, W. van Gunsteren, J. Hermans, et al., Interaction models for water in relation to protein hydration, in: Intermolecular Forces, D. Reidel Publishing Company, 1981, pp. 331–342.
[30] S. Aibara, M. Kato, M. Ishinaga, M. Kito, Changes in positional distribution of fatty acids in the phospholipids of *Escherichia coli* after shift-down in temperature, BBA - Lipid Lipid Metab. 270 (1972) 301–306.
[31] M. Kito, M. Ishinaga, M. Nishihara, M. Kato, T. Hata, S. Sawada, Metabolism of the phosphatidylglycerol molecular species in *Escherichia coli*, Eur. J. Biochem. 54 (1975) 55–63.
[32] K. Yokota, R. Kanamoto, M. Kito, Composition of cardiolipin molecular species in *Escherichia coli*, J. Bacteriol. 141 (1980) 1047–1051.
[33] A. Kukol, Lipid models for united-atom molecular dynamics simulations of proteins, J. Chem. Theory Comput. 5 (2009) 615–626.
[34] N. Guex, M.C. Peitsch, SWISS-MODEL and the Swiss-Pdb viewer: an environment for comparative protein modeling, Electrophoresis 18 (1997) 2714–2723.
[35] M.G. Wolf, M. Hoefling, C. Aponte-Santamaría, H. Grubmüller, G. Groenhof, g_membed: efficient insertion of a membrane protein into an equilibrated lipid bilayer with minimal perturbation, J. Comput. Chem. 31 (2010) 2169–2174.
[36] S. Nosé, A molecular dynamics method for simulations in the canonical ensemble, Mol. Phys. 52 (1984) 255–268.
[37] W.G. Hoover, Canonical dynamics: equilibrium phase-space distributions, Phys. Rev. A 31 (1985) 1695.
[38] S. Nosé, M.L. Klein, Constant pressure molecular dynamics for molecular systems, Mol. Phys. 50 (1983) 1055–1076.
[39] M. Parrinello, A. Rahman, Polymorphic transitions in single crystals: a new molecular dynamics method, J. Appl. Phys. 52 (1981) 7182–7190.
[40] U. Essmann, L. Perera, M. Berkowitz, T. Darden, H. Lee, L. Pedersen, A smooth particle mesh Ewald method, J. Chem. Phys. 103 (1995) 8577–8593.
[41] B. Hess, P-LINCS: a parallel linear constraint solver for molecular simulation, J. Chem. Theory Comput. 4 (2007) 116–122.
[42] M. Valiev, E.J. Bylaska, N. Govind, K. Kowalski, T.P. Straatsma, H.J.J. Van Dam, D. Wang, J. Nieplocha, E. Apra, T.L. Windus, W.A. de Jong, NWChem: a comprehensive and scalable open-source solution for large scale molecular simulations, Comput. Phys. Commun. 181 (2010) 1477–1489.
[43] C. Kandt, Z. Xu, D.P. Tieleman, Opening and closing motions in the periplasmic vitamin B12 binding protein BtuF, Biochemistry 45 (2006) 13284–13292.
[44] A.D. Becke, Density-functional thermochemistry. III. The role of exact exchange, J. Chem. Phys. 98 (1993) 5648–5652.
[45] C. Lee, W. Yang, R.G. Parr, Development of the Colle–Salvetti correlation-energy formula into a functional of the electron density, Phys. Rev. B 37 (1988) 785–789.
[46] P.J. Hay, W.R. Wadt, Ab initio effective core potentials for molecular calculations. Potentials for the transition metal atoms Sc to Hg, J. Chem. Phys. 82 (1985) 270–283.
[47] A. Zinelabidine, A. Bouraoui, F. Mhenni, B. Blaive, R. Gallo, Molecular mechanics modelling of siderophores, J. Mol. Struct. (THEOCHEM) 286 (1993) 267–274.
[48] G. Xiao, D. van der Helm, R.C. Hider, B.L. Rai, Molecular modeling studies of a ferric hexadentate 3-hydroxy-2(1H)-pyridinone complex and an analogue by molecular mechanics, molecular dynamics, and free energy perturbation simulations, J. Phys. Chem. US 100 (1996) 2345–2352.
[49] R Development Core Team, R: A Language and Environment for Statistical Computing, 2008.
[50] W. Kabsch, C. Sander, Dictionary of protein secondary structure: pattern recognition of hydrogen-bonded and geometrical features, Biopolymers 22 (1983) 2577–2637.
[51] W. Humphrey, A. Dalke, K. Schulten, VMD: visual molecular dynamics, J. Mol. Graphics 14 (1996) 33–38.
[52] H. Flyvbjerg, H.G. Petersen, Error estimates on averages of correlated data, J. Chem. Phys. 91 (1989) 461–466.

[53] A. Grossfield, D.M. Zuckerman, Chapter 2 quantifying uncertainty and sampling quality in biomolecular simulations, in: A.W. Ralph (Ed.), Annu. Rep. Comput. Chem., vol. 5, Elsevier, 2009, pp. 23–48.
[54] B. Hess, Convergence of sampling in protein simulations, Phys. Rev. E 65 (2002) 031910.
[55] J.D. Faraldo-Gómez, L.R. Forrest, M. Baaden, P.J. Bond, C. Domene, G. Patargias, J. Cuthbertson, M.S.P. Sansom, Conformational sampling and dynamics of membrane proteins from 10-nanosecond computer simulations, Proteins 57 (2004) 783–791.
[56] A. Grossfield, S.E. Feller, M.C. Pitman, Convergence of molecular dynamics simulations of membrane proteins, Proteins 67 (2007) 31–40.
[57] T.D. Romo, A. Grossfield, Block covariance overlap method and convergence in molecular dynamics simulation, J. Chem. Theory Comput. 7 (2011) 2464–2472.
[58] D.P. Tieleman, H.J.C. Berendsen, A molecular dynamics study of the pores formed by *Escherichia coli* OmpF porin in a fully hydrated palmitoyloleoylphosphatidylcholine bilayer, Biophys. J. 74 (1998) 2786–2801.
[59] J.D. Faraldo-Gómez, G.R. Smith, M.S.P. Sansom, Molecular dynamics simulations of the bacterial outer membrane protein FhuA: a comparative study of the ferrichrome-free and bound states, Biophys. J. 85 (2003) 1406–1420.
[60] S. Khalid, M.S.P. Sansom, Molecular dynamics simulations of a bacterial autotransporter: NalP from *Neisseria meningitidis*, Mol. Membr. Biol. 23 (2006) 499–508.
[61] S. Khalid, P.J. Bond, T. Carpenter, M.S.P. Sansom, OmpA: gating and dynamics via molecular dynamics simulations, BBA - Biomembr. 1778 (2008) 1871–1880.
[62] J. Gumbart, M.C. Wiener, E. Tajkhorshid, Coupling of calcium and substrate binding through loop alignment in the outer-membrane transporter BtuB, J. Mol. Biol. 393 (2009) 1129–1142.
[63] S.S. Deol, P.J. Bond, C. Domene, M.S.P. Sansom, Lipid–protein interactions of integral membrane proteins: a comparative simulation study, Biophys. J. 87 (2004) 3737–3749.
[64] N. Schmid, A. Eichenberger, A. Choutko, S. Riniker, M. Winger, A. Mark, W. van Gunsteren, Definition and testing of the GROMOS force-field versions 54A7 and 54B7, Eur. Biophys. J. 40 (2011) 843–856.
[65] W. Huang, Z. Lin, W.F. van Gunsteren, Validation of the GROMOS 54A7 force field with respect to β-peptide folding, J. Chem. Theory Comput. 7 (2011) 1237–1243.
[66] T.P. Straatsma, T.A. Soares, Characterization of the outer membrane protein OprF of *Pseudomonas aeruginosa* in a lipopolysaccharide membrane by computer simulation, Proteins 74 (2009) 475–488.
[67] S. Khalid, P.J. Bond, S.S. Deol, M.S.P. Sansom, Modeling and simulations of a bacterial outer membrane protein: OprF from *Pseudomonas aeruginosa*, Proteins 63 (2006) 6–15.
[68] A. Laio, M. Parrinello, Escaping free-energy minima, Proc. Natl. Acad. Sci. 99 (2002) 12562–12566.
[69] M. Kim, G.E. Fanucci, D.S. Cafiso, Substrate-dependent transmembrane signaling in TonB-dependent transporters is not conserved, Proc. Natl. Acad. Sci. 104 (2007) 11975–11980.
[70] J. Yang, L. Aslimovska, C. Glaubitz, Molecular dynamics of proteorhodopsin in lipid bilayers by solid-state NMR, J. Am. Chem. Soc. 133 (2011) 4874–4881.
[71] P.J.R. Spooner, R.H.E. Friesen, J. Knol, B. Poolman, A. Watts, Rotational mobility and orientational stability of a transport protein in lipid membranes, Biophys. J. 79 (2000) 756–766.
[72] T.J. Piggot, Á. Piñeiro, S. Khalid, Molecular dynamics simulations of phosphatidylcholine membranes: a comparative force field study, J. Chem. Theory Comput. 8 (11) (2012) 4593–4609.